Video Article

Simulation, Fabrication and Characterization of THz Metamaterial Absorbers

James P. Grant[1], Iain J.H. McCrindle[1], David R.S. Cumming[1]

[1]School of Engineering, University of Glasgow

Correspondence to: David R.S. Cumming at david.cumming.2@glasgow.ac.uk

Abstract

Metamaterials (MM), artificial materials engineered to have properties that may not be found in nature, have been widely explored since the first theoretical[1] and experimental demonstration[2] of their unique properties. MMs can provide a highly controllable electromagnetic response, and to date have been demonstrated in every technologically relevant spectral range including the optical[3], near IR[4], mid IR[5], THz[6], mm-wave[7], microwave[8] and radio[9] bands. Applications include perfect lenses[10], sensors[11], telecommunications[12], invisibility cloaks[13] and filters[14,15]. We have recently developed single band[16], dual band[17] and broadband[18] THz metamaterial absorber devices capable of greater than 80% absorption at the resonance peak. The concept of a MM absorber is especially important at THz frequencies where it is difficult to find strong frequency selective THz absorbers[19]. In our MM absorber the THz radiation is absorbed in a thickness of ~ $\lambda/20$, overcoming the thickness limitation of traditional quarter wavelength absorbers. MM absorbers naturally lend themselves to THz detection applications, such as thermal sensors, and if integrated with suitable THz sources (*e.g.* QCLs), could lead to compact, highly sensitive, low cost, real time THz imaging systems.

Video Link

The video component of this article can be found at https://www.jove.com/video/50114/

Introduction

This protocol describes the simulation, fabrication and characterization of single band and broadband THz MM absorbers. The device, shown in **Figure 1**, consists of a metal cross and a dielectric layer on top of a metal ground plane. The cross-shaped structure is an example of an electric ring resonator (ERR)[20,21] and couples strongly to uniform electric fields, but negligibly to a magnetic field. By pairing the ERR with a ground plane, the magnetic component of the incident THz wave induces a current in the sections of the ERR that are parallel to the direction of the E-field. The electric and magnetic response can then be tuned independently and the impedance of the structure matched to free space by varying the geometry of the ERR and the distance between the two metallic elements. As shown in **Figure 1(d)**, the symmetry of the structure results in a polarization insensitive absorption response.

Protocol

1. Simulation of a Single Band THz Metamaterial Absorber

A 3D view of the simulation set-up is shown in **Figure 2**.

1. Lumerical FDTD is used to optimize the transmission, reflection and absorption characteristics of the THz metamaterial absorber. All units are given in μm.
2. Define the THz polyimide material properties by left clicking *Materials, Add (n,k) material* and inputting 1.68 as the n and 0.06 as the k. Double left click on "new material 1" and rename it as "polyimide". Note that if theoretical or experimental refractive index data is available one can "*add sampled data"* to define the material properties.
3. Draw the geometry of the device, starting with the 0.2 μm thick metal ground plane. In the *structures* tab select *rectangle* and edit the properties by pressing the *e* key. Input "groundplane" in the *name* window, (0,0,0.1) as the structure centre co-ordinates and (31,31,0.2) as the span region. Move to the *material* tab and select *Perfect Electrical Conductor (PEC)*. Repeat to define the 3 μm thick polyimide dielectric layer typing "polyimide" in the name window, (0,0,1.7) as the centre co-ordinates and (31,31,3) as the span. Finally define the 0.2 μm thick electric ring resonator by drawing two rectangular *Perfect Electrical Conductor (PEC)* regions called "ERR arm1" and "ERR arm2" with the same centre co-ordinates of (0,0,3.3) but different span regions of (10,26,0.2) and (26,10,0.2) respectively.
4. Add the simulation region by left clicking on *Simulation* and press *e* to edit the properties. In the *general tab* input 20 psec as the simulation time. In the *geometry tab* choose (0,0,0) as the centre co-ordinates and (30,30,200) as the span regions. In the *mesh settings* tab select a mesh accuracy of 3 and keep the other default settings as they are. Set the simulation boundary conditions in the *boundary conditions* tab

choosing "Anti-symmetric" for x min bc and x max bc, "symmetric" for y min bc and y max bc and "PML" for z min bc and z max bc (the "allow symmetry on all boundaries" must be ticked). Include a mesh override region by left clicking again on *Simulation* and edit by pressing e. In the *general* tab type 0.5 µm for the dx and dy override and 0.05 µm for the dz override. In the *geometry* tab enter the centre co-ordinates (0,0,1.7) and span regions (30,30,3.8). Note that a smaller mesh size of *e.g.* dx, dy 0.1 µm, will increase simulation accuracy though this will come at the expense of significantly increased CPU memory and simulation time. It is best to simulate using a large mesh size until a structure with the desired properties is obtained and then re-simulate using the smaller mesh size.

5. Define the source type by left clicking on the arrow next to *sources* and choosing *plane wave*. Press e to edit the source properties and in the *general* tab change the direction to backward. In the geometry tab enter the centre co-ordinates (0,0,90) and (35,35,0) for the span region. Note that you cannot modify the z span. Set the minimum and maximum frequency of the simulation in the *frequency/wavelength* tab. Choose a minimum of 1 THz and a maximum of 4 THz and ensure the pulse in the signal versus time graph in the bottom right corner of the window decays to zero well before 20 psec.

6. Left click on the arrow next to *Monitors* and select *frequency-domain field profile*. Press e to edit the monitor properties and enter "r95" in the *monitor name* window. In the *geometry tab* enter the centre co-ordinates of (0,0,95) and span region (30,30,0). Repeat and create a second *frequency-domain field profile* monitor called "t95" with centre co-ordinates (0,0,-95) and spans (30,30,0). Left click on the arrow next to *Monitors* and select *global properties*. In the *frequency/power profile* tab enter 100 in the frequency points window. **Figure 2** shows the perspective view displayed in Lumerical on completion of steps 1.1-1.6. Check the memory requirements are compatible with your computer by left clicking on the arrow next to the *Check* icon on the top toolbar and selecting *check simulation memory requirements*. Save the file giving it an appropriate name such as "Jove.sim".

7. Run the simulation by left clicking on the *Run* icon.

8. On completion of the simulation enter the following into the *script prompt* window. Note that one can also enter the following text in a text editor and save the file as a .lsf file. The script can then be run by left clicking on the arrow next to *Run*, selecting *script* and then locating the script file saved on your computer. Note that the # symbol indicates a comment.

```
load("Jove_sim"); # loads the simulation file
f = getdata("r95","f"); # gets the reflection data and frequency data from the r95 monitor
R = transmission("r95"); # defines R as a matrix containing the reflection data
A = 1-R; # calculates the absorption
fthz=f/1e12; # converts frequency to THz
plot(fthz,A,R,"Frequency(THz)","Absorption","Reflection"); # plot data on a single graph
legend("Absorption","Reflection");
filename = "Jove_sim.csv"; # export data for excel import
rm(filename); # delete file if it already exists
lambda = c/f; # converts frequency to wavelength
for(i=1:length(lambda)) {
  write(filename,num2str(f(i)) + "," + num2str(fthz(i)) + "," + num2str(R(i)) + "," + num2str(A(i)) + "," );
} # outputs a .csv file in column format of the frequency, reflection and absorption
```

2. Fabrication of a Single Band THz Metamaterial Absorber

Figure 3 shows the most important fabrication steps.

1. Clean a 15 mm by 15 mm piece of silicon in sequential solutions of warm (50 °C) opticlear, acetone and isopropanol using ultrasonic agitation after initially heating the beaker containing the solvent for 10 min. Note that this protocol can also be used to fabricate several devices onto a 4 inch diameter wafer.

2. Evaporate a metal bi-layer of 20 nm/100 nm Ti/Au onto the 15 mm by 15 mm using a Plassys 450 MEB electron beam evaporator (**Figure 3, step 1**). Note that the metal thickness must be greater than the skin depth at the desired operating frequency.

3. Clean the sample as previously described in section 2.1

4. Dispense VM651 primer onto the sample using a pipette and leave to relax for 20 sec. Spin sample at 4,000 rpm for 5 sec and then bake on a contact hotplate at 120 °C for 60 sec.

5. Remove Dupont PI2545 polyimide from the freezer. Allow 20 min for the bottle to reach room temperature. This is essential since opening the bottle directly after removal from the freezer will result in moisture condensing inside the bottle and degrading the polyimide film properties. Dispense PI2545 onto the sample using a pipette and allow 20 sec for it to relax. Spin sample using a 2 stage spin procedure with the following settings - (i) final spin speed 500 rpm, acceleration 100 rpms^{-1}, final spin time 5 sec (ii) final spin speed 6,000 rpm, acceleration 500 rpms^{-1}, final spin time 60 sec. Bake sample on a contact hotplate at 140 °C for 5 min (**Figure 3, step 2**). If a thicker polyimide film is required then either spin multiple layers or reduce the final spin speed. To obtain a polyimide film thickness of 3 µm with minimal edge bead three layers of PI2545 are spun using the above protocol.

6. Cure the polyimide on a contact hotplate at 220 °C for 10 min. After this cure procedure the PI2545 will be impervious to most solvents and acids and can only be removed using oxygen plasma. PI2545 can be spun onto a dummy piece of silicon, cured as above and the thickness of the film measured by scratching the polyimide and using a DEKTAK surface profilometer to measure the step height.

7. Deposit 15% 2010 Poly(methyl methacrylate), known as PMMA, onto the sample. Spin at 5,000 rpm for 60 sec and bake in a convection oven at 180 °C for 30 min. Before baking remove any excess resist that has crept on to the backside of the sample using acetone. Remove sample from the oven and leave to cool to room temperature (~5 min). Deposit 4% 2041 PMMA onto the sample, spin at 5,000 rpm for 60 sec and bake in a convection oven at 180 °C for 60 min (**Figure 3, step 3**). Remove any excess resist that has crept on to the backside of the sample using acetone before baking.

8. Write the desired job on a Vistec VB6 electron beam writer using a dose of 450 µC/cm^2. The job file is designed in Tanner L-Edit, fractured into polygons by Layout Beamer and finally submitted to the beam writer using the Java based BELLE software.

9. Develop the sample in a solution of 1:1 MIBK:IPA at a temperature of 23 °C for 60 sec (**Figure 3, step 4**). Rinse in a beaker of isopropanol. Inspect pattern fidelity on an optical microscope. If features are poorly resolved strip the resist in opticlear, acetone and isopropanol and start again from 2.2.

10. Descum the sample with O_2 using a Gala Plasmaprep$_5$ barrel asher for 1 min at 0.1 mbar and 50 W RF power. Evaporate 20 nm Ti and 150 nm Au using a Plassys 450 MEB electron beam evaporator (**Figure 3, step 5**).
11. Insert the sample into a beaker of warm acetone and place the beaker into a hot water bath kept at 50 °C. After 4 hr remove the sample from the water bath and using a pipette suck up some of the warm acetone and spray liberally onto the sample (**Figure 3, step 6**). Inspect sample by eye to check that metal is lifting off from the areas where PMMA was present. If lift-off is progressing slowly place beaker in the ultrasonic water bath for 2 min. Inspect sample under the optical microscope.
12. The protocol describes the fabrication of a single band THz absorber however multi-level dual band and broadband absorbers can be produced by repeating steps 2.3-2.11 and stacking several crosses on top of polyimide layers.

3. Characterization of a Single Band THz Metamaterial Absorber

Figure 4 shows the basic FTIR instrument layout.

1. Turn on the nitrogen supply to the IFS 66V/S Fourier Transform Infra Red (FTIR) spectrometer. Press the "FIR" button on the front of the spectrometer control unit to turn on the Hg arc lamp. It takes around 15 min for the lamp power to stabilize. Insert the 6 µm multilayer beam splitter into the appropriate slot in the interferometer unit.
2. Vent the sample compartment of the spectrometer and insert the PIKE 30 ° reflection unit. Place the 4 mm aperture on top of the reflection unit aperture and on top of this put a gold mirror. The 4 mm aperture determines the area of the sample that will be interrogated while the gold mirror is necessary to make a background measurement.
3. Evacuate the sample compartment and wait for the pressure to get down to 5 mbar. The spectrometer can be run in a purged nitrogen environment however the signal size typically drops to less than 20% compared to vacuum.
4. Start the OPUS software and load the configuration file (set-up on installation of the unit) for taking measurements in the 30 cm^{-1} to 300 cm^{-1} range (1-9THz). This file sets numerous spectrometer parameters such as the scanner velocity, source aperture, source type, data collection method and Fourier transform execution mode. Ensure the LED on the front of the detector compartment is flashing green, indicating that the scanner is operating. Check that the shape of the interferogram is as expected.
5. Run 100 background scans to obtain the background spectrum.
6. Vent sample compartment, remove mirror and place sample face down onto the aperture. Ensure the centre of the sample is in the middle of the aperture. Evacuate the sample compartment.
7. Run 1,000 sample scans to obtain the sample spectrum. The sample spectrum will be compared to the background reference spectrum and the final reflection spectrum of the sample obtained. Note that if the signal reaching the detector is low, a greater number of sample scans may be required to reduce the noise (*e.g.* 10,000 scans). Repeat sample scans should be made to ensure the measured data is reliable and consistent.
8. Data from the completed scan can be converted into a text file and analyzed offline. The continuous ground plane of the sample means that there is no transmission ergo the absorption spectrum can be found by subtracting the reflection from 1.

Representative Results

Figure 5(a) shows the experimentally obtained and simulated absorption spectra for a MM absorber with a 3.1 µm thick polyimide dielectric spacer. This MM structure has a repeat-period of 27 µm and dimensions K = 26 µm, L = 20 µm, M = 10 µm and N = 5 µm. Experimental measurements were also performed on samples with no ERR layer to confirm that absorption was a consequence of the MM structure and not of the dielectric. The 7.5 µm thick polyimide sample with no ERR structure has a maximum absorption of 5 % across the frequency range of interest, see **Figure 5(a)**, thereby verifying that at the resonance frequency absorption is a result of the MM structure. The experimental data shows a resonance peak at 2.12 THz of 77% absorption magnitude. This result is in excellent agreement with the simulated absorption maximum of 81% at 2.12 THz. **Figure 5(b)** shows the experimental data for MM absorbers with the same ERR geometry for different polyimide thicknesses ranging from 1-7.5 µm and for an absorber where the dielectric is 3 µm of SiO_2. As the polyimide thickness increases from 1 µm to 3.1 µm the peak absorption increases, but at polyimide thicknesses greater than 3.1 µm there is a slight reduction in the peak absorption value. A distinct red-shift of 0.25 THz is observed as the polyimide thickness increases from 1 µm to 7.5 µm. Absorbers that had SiO_2 as the dielectric instead of polyimide were also studied. A maximum absorption value of 65% at 1.90 THz was measured for such a MM absorber with a 3 µm thick SiO_2 dielectric layer.

The effective permittivity and permeability can be extracted from the simulated data via inversion of the S parameters[22]. The retrieved parameters for the simulated MM absorber with a 3.1 µm thick polyimide spacer are displayed in **Figure 5(c).** As can be observed the real parts of the optical constants cross close to zero - a condition required for zero reflection, while whenever the real part of the permittivity is positive the real part of the permeability is negative and vice versa - a condition required for zero transmission. At the frequency of maximum absorption, ω_0, there is a peak of the imaginary component of the permeability implying high absorption.

Lumerical FDTD can also be used to establish the location of the absorption within the MM structure. The simulated power absorption distributions for the ERR, dielectric and the ground plane layers are shown in **Figures 6(a-c)** while a cross-section of the power distribution in the xz plane at y = 3 µm is shown in **Figure 6(d)**. From these plots it is clear that the majority of the energy is dissipated as Ohmic loss in the ERR layer and as dielectric loss in the first 500 nm of polyimide below this layer. The regions of maximum absorption loss occur between adjacent unit cells and around the inner edges of the cross.

Parameter	p	L1	L2	L3	h1	h2	h3
Value (mm)	22	17	15.4	15	0.7	1.2	2.0

Table 1. Geometric parameters of the multi-layer absorber.

Metamaterial absorbers are inherently narrowband devices; the bandwidth typically being no more than 20% of the centre resonant frequency. Several applications, such as THz spectroscopy, require sensors that exhibit broadband THz absorption. We have developed two strategies to

realize such broadband absorption. The first, depicted in **Figure 7(a-c)** is to stack alternating layers of metallic ERRs and dielectric layers on top of a continuous ground plane. In different layers we design crosses of differing lengths (L_1 - L_3) in order to support several resonant modes closely positioned together in the absorption spectrum. By tuning the dielectric thickness (h_1 - h_3) the multi-layer structure can be impedance-matched to free space at each resonant frequency and broadband absorption obtained. A standard electron beam registration process is used to align the ERRs on top of one another. Our second strategy is to incorporate four ERRs into a four "colour" super-pixel, see **Figure 7(d),** onto a single dielectric layer *i.e.* ground plane/dielectric/metallic ERRs. Such a device is much simpler to fabricate than the multi-layer absorber.

The experimentally obtained absorption spectrum and the simulated data for a multi-layer MM absorber, with dimensions stated in **Table 1**, are shown in **Figure 8(a)**. Also plotted is the experimentally obtained absorption spectrum for a single ERR of arm length 17 μm and dielectric thickness of 2 μm. The one layer structure has a single resonance peak at 5.42 THz where 78 % of the EM radiation is absorbed. In contrast, the 3-layer device has three resonances at 4.32, 5.31 and 5.71 THz with absorption magnitudes of 66 %, 77 % and 80 % respectively. Owing to these three closely position resonant peaks we obtain a wide frequency band, from 4.08 THz to 5.94 THz, where the absorption is greater than 60 %. Taking the central frequency of the 3-layer structure to be 5.01 THz the full width half maximum (FWHM) of the absorption is 48 % of the central frequency. This is almost two and a half times the FWHM of the single layer structure (FWHM of the single layer is 20 %). The experimental data is in reasonable agreement with the simulated spectrum.

To understand the origin of the spectral characteristics the simulated absorption distributions in the x-z plane of the three resonances are plotted in **Figure 9** (a-c). The resonance at 4.84 THz is primarily associated with excitation of the bottom ERR layer while the resonances at 5.16 THz and 5.70 THz are mainly a consequence of excitation of the middle and top ERR layers respectively. These distributions clearly reveal that each ERR contributes to the broadband absorption.

An SEM image of a four colour super-pixel THz absorber is shown in **Figure 7(d). Figure 8(b)** shows the simulated and experimental absorption spectra for a super-pixel with arm lengths of 17 μm, 15 μm, 13 μm and 11 μm and arm widths of 6 μm. The pixel period is 44 μm while the polyimide thickness is 2 μm. Four resonances are observed in both the simulation and experimental data. The disadvantage of such a super-pixel structure is that, as shown in **Figure 8(b)**, there is some polarization dependence. For both polarizations the super-pixel absorber has greater than 50% absorption between 5.08 and 7.27 THz; a range of 2.19 THz. The FWHM for TE polarization is 37% while it is 41% for TM polarization, representing double the FWHM of the single pixel.
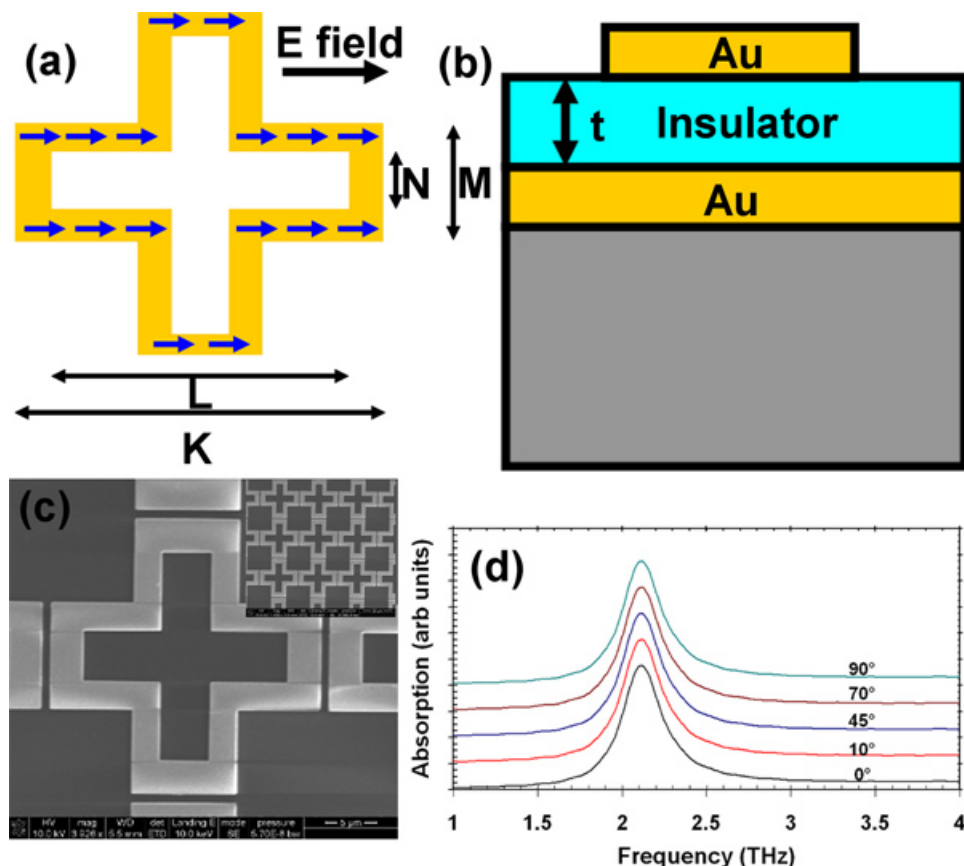

Figure 1. (a) Schematic of the ERR of the MM absorber and (b) cross-section of complete MM absorber. A current is induced in the sections of the ERR that are parallel to the E field (direction denoted by blue arrows in (a). An anti-parallel image current flows in the regions of the ground plane imemdiately below the cross, resulting in a resonant response. (c) SEM image of the unit cell and (inset) section of the array. (d) Simulated absorption spectra for different incident polarization angles showing polarization insensitivity of the MM absorber. Each successive plot from 0-90 ° is offset by one major unit of the ordinate axis.
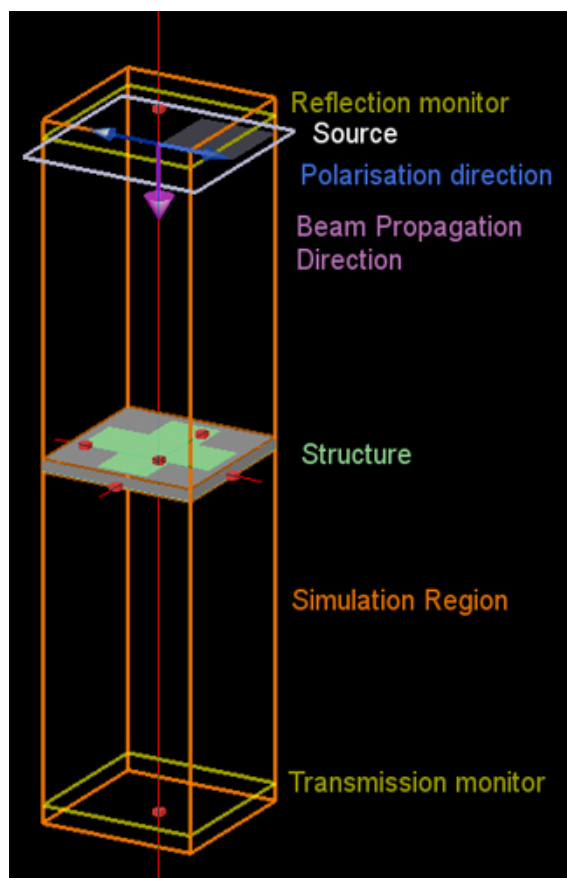
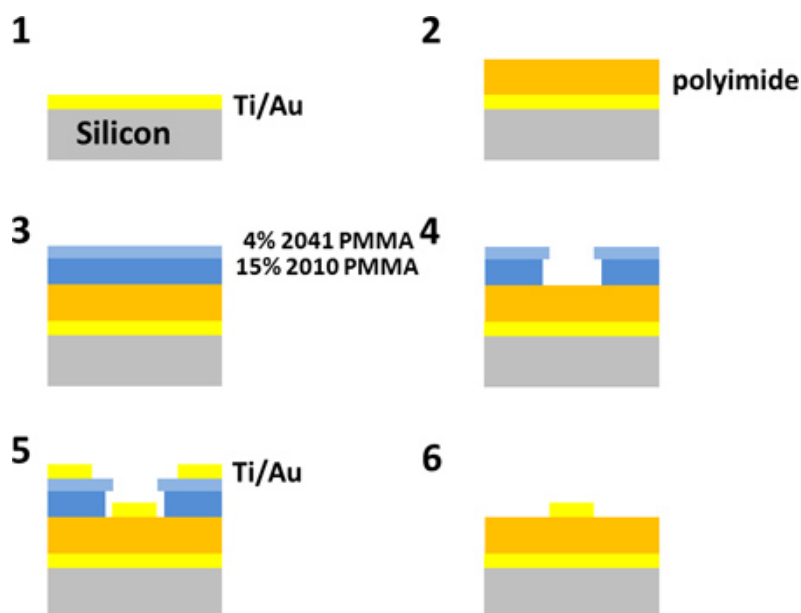**Figure 2.** 3D Schematic of the simulation set-up.

Figure 3. Fabrication of single band MM absorber. 1) A 20 nm/100 nm Ti/Au stack is evaporated onto a 15 mm by 15 mm section of silicon. 2) PI2545 is spin coated onto the sample, baked at 140 °C and then cured at 220 °C. 3) A bi-layer of 15% 2010 and 4% 2041 is spin coated and baked at 180 °C. 4) After exposure to a 100 keV electron beam the sample is developed in a solution of MIBK and IPA. The 2010 PMMA, owing to its lower molecular weight, develops faster than the 2041 PMMA. This results in the desired overhang profile required to attain successful lift-off. 5) A 20 nm/150 nm Ti/Au film is evaporated onto the sample. 6) Unwanted regions of metal are lifted-off by immersing the sample in a beaker of warm acetone.
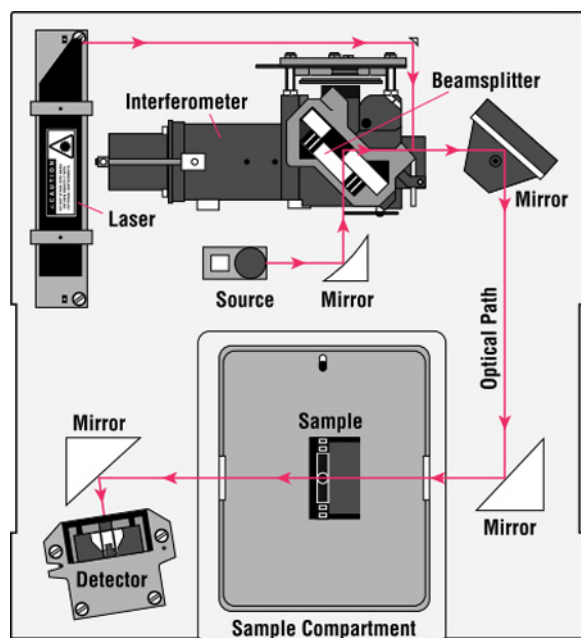
Figure 4. Schematic of a Fourier Transform Infrared Spectrometer[27].
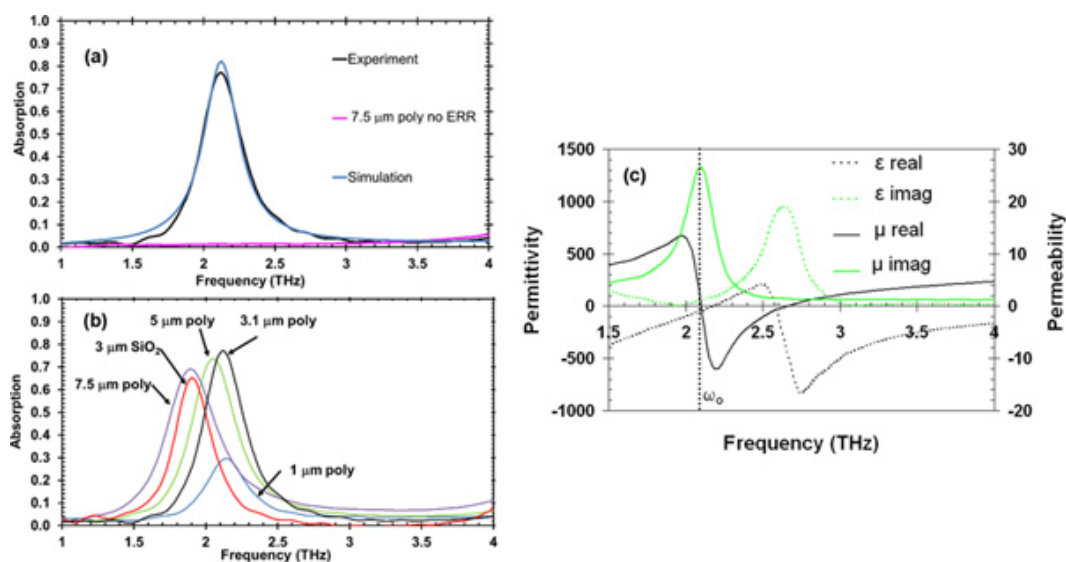

Figure 5. (a) Experimental and simulated data of a MM absorber with a polyimide thickness of 3.1 µm. Also plotted is the absorption of a 7.5 µm thick polyimide film. (b) Experimental absorption spectra for MMs with differing dielectric spacer thickness and type. (c) Extracted optical parameters from the simulated 3.1 µm thick polyimide MM absorber. Click here to view larger figure.
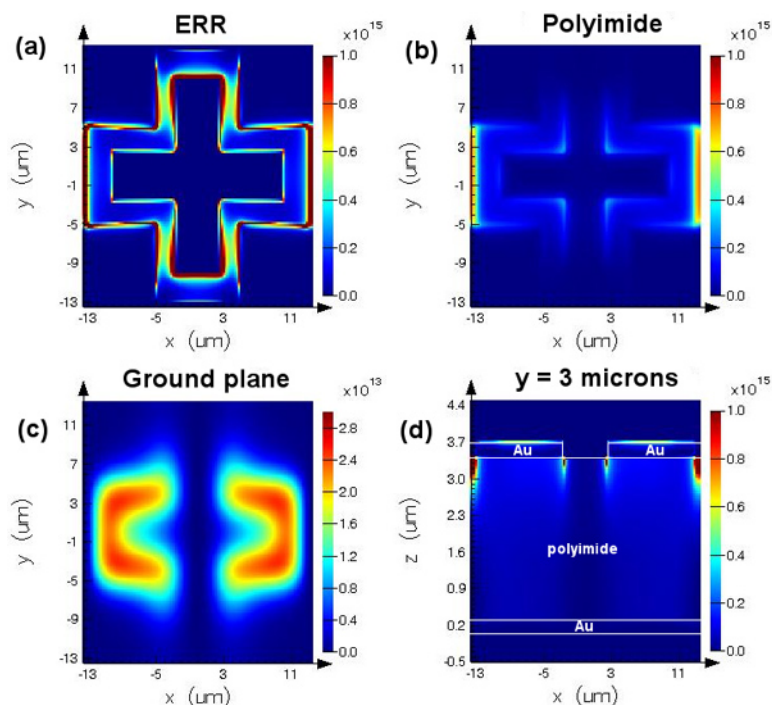
Figure 6. Energy dissipation in a MM absorber structure with a 3.1 µm thick polyimide spacer at a frequency of 2.12 THz. Energy dissipation in (a) the ERR layer, (b) the centre of the polyimide, (c) the ground plane and (d) xz plane at y = 3 µm.
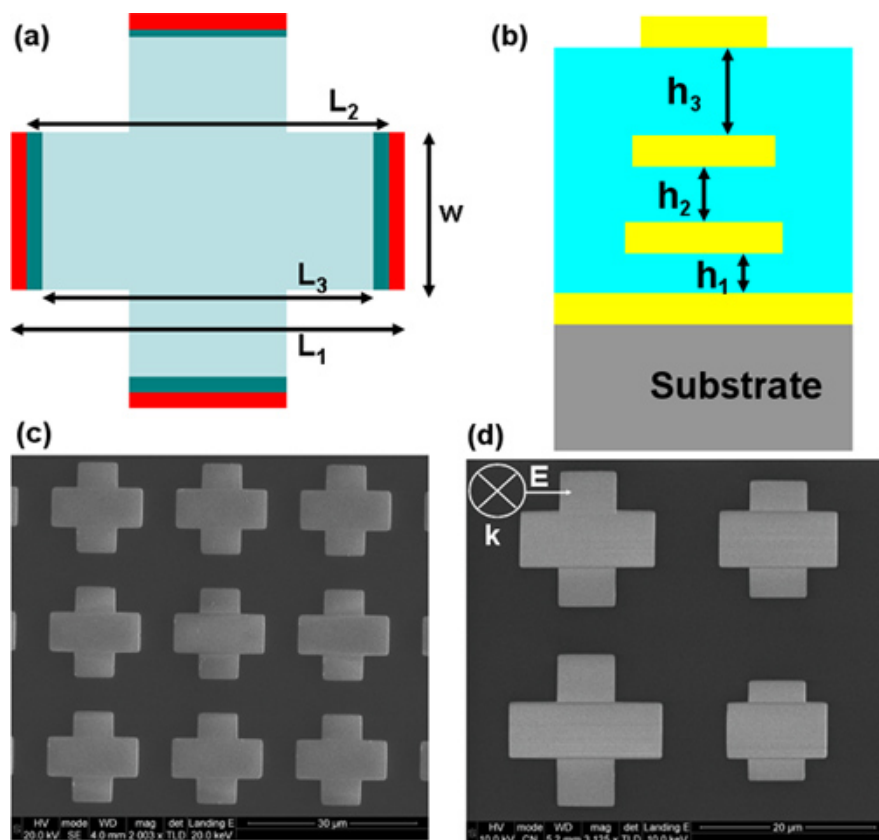

Figure 7. (a) Plan view of the 3-layer MM absorber and (b) cross-section of the complete device. (c) SEM image of 9 unit cells of the multi-layer absorber and (d) SEM image of a single 'super-pixel' broadband absorber. The orientation for TE polarization is shown in the inset.
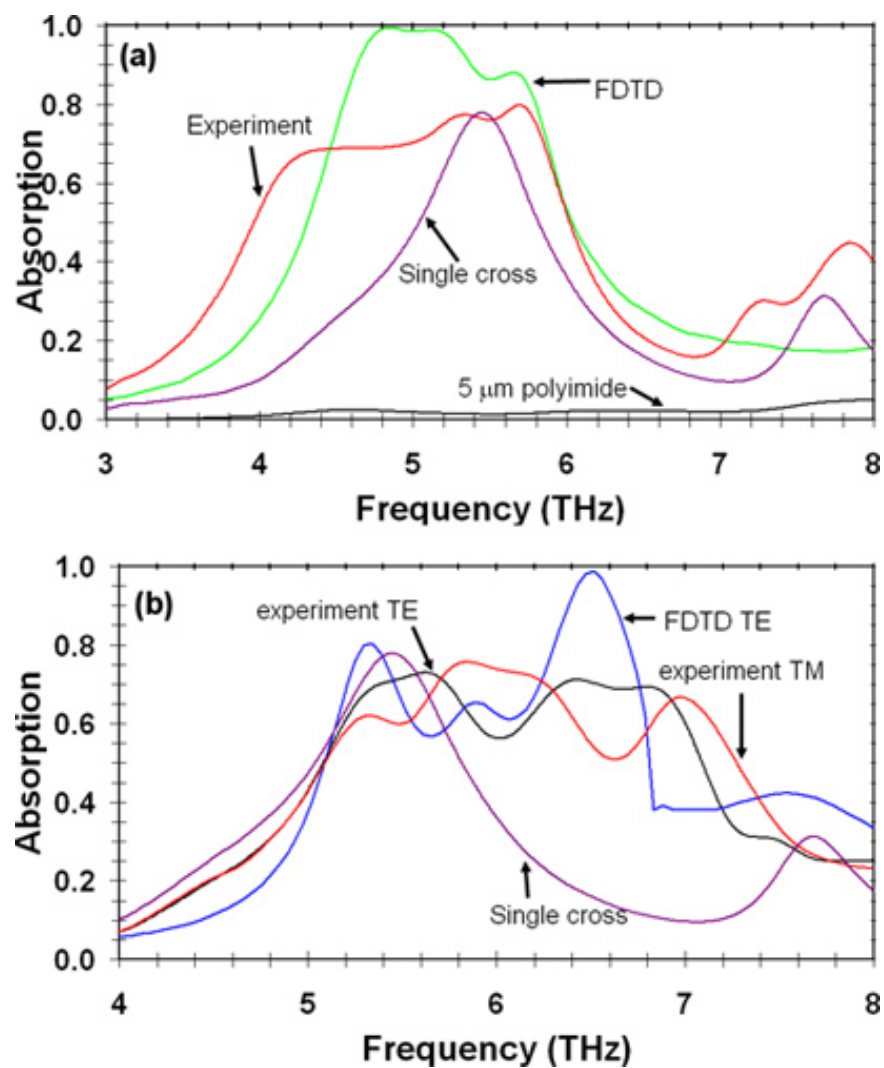
Figure 8. (a) Experimental and simulated (FDTD) data of the multi-layer absorber. Also plotted is the experimental absorption spectrum for a single layer absorber. (b) Absorption spectra for the 'super-pixel' broadband absorber.
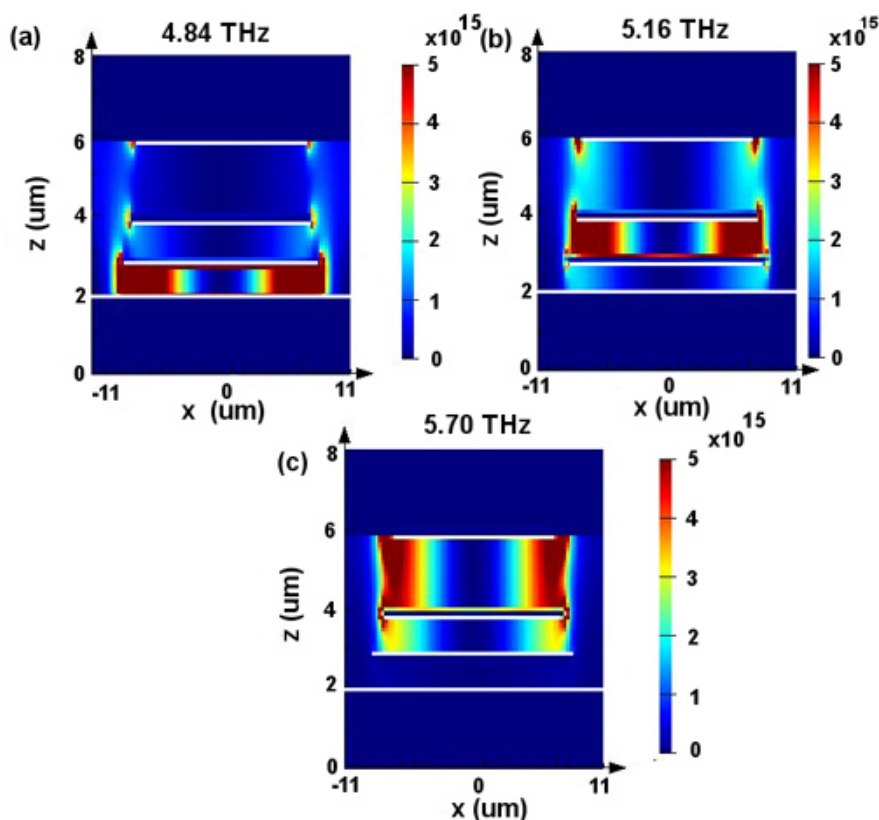
Figure 9. (a-c) Absorption distribution in the x-z plane at y = 0 μm at the three resonant frequencies. The horizontal white lines denote Au layers.

Discussion

This protocol describes the simulation, fabrication and characterization of THz metamaterial absorbers. It is essential such sub-wavelength structures are accurately simulated before any effort is committed to costly fabrication procedures. Lumerical FDTD simulations provide information on not only the MM absorption spectrum but also the location of the absorption, essential knowledge to aid placement of a transducer and obtain the maximum response. In addition the optimization algorithm in Lumerical can be implemented to rapidly establish an appropriate absorber structure for a pre-defined figure of merit (e.g. frequency position, absorption maximum, absorption minimum, bandwidth etc). Simulation, fabrication and characterization of a single band MM absorber can be completed in less than 24 hr allowing rapid prototyping of any design. Our multi-layer broadband absorber consists of three separate electron beam write steps (two registration steps) and could be realized in less than 4 days. We have also fabricated absorbers which have SiO_2 and Si_3N_4 insulating regions between the ERR and the ground plane. These layers were deposited by PECVD and ranged in thickness between 0.6 and 3 μm. The absorption magnitudes were similar to devices with polyimide dielectric layers however there was a red shift in the frequency position for absorbers of the same thickness.

The beauty of metamaterials is their inherent scalability - absorber structures have been demonstrated from the mm[23] region through to infrared and optical frequencies[24]. These devices consist of the standard metallic ERR/insulator/metallic structure with the appropriate ERR feature size and insulator type and thickness. In our design the resonant frequency position is mainly dependent on the period, cross arm length of the structure and insulator type while the absorption magnitude is determined by the thickness of the insulating layer. The resonant frequency position of our cut-out cross design is blue shifted compared to more traditional whole cross designs (no-cut out sections). This allows the pixel period to be reduced for a particular targeted resonant frequency (e.g. 2.52 THz) and has important implications for THz imaging applications. A major advantage of our device is that in contrast to more complex and computationally intensive ERR geometries our ERR geometry is simple to understand and computationally undemanding. While we use effective medium theory to describe our metamaterial absorbers, a different explanation centering on interference theory has recently been proposed[25].

Research into THz radiation, with wavelengths between 30 μm and 3 mm, has burgeoned in the last decade. This interest has been stimulated by the unique properties of THz rays; they can penetrate materials such as plastics, paper and many organic compounds, including human tissue, without the hazards or potential dangers associated with ionising radiation such as x-rays. Furthermore, THz may be used to identify specific materials via their characteristic spectra, including explosives, hazardous chemicals, drugs and DNA, as molecular rotations and vibrations occur in this wavelength range. Accordingly THz imaging has found applications in areas such as security, healthcare, pharmaceuticals, automotive, materials science and non-destructive testing.

However there are many unfulfilled opportunities owing to the lack of low-cost, compact and easily deployable equipment. Present THz imaging systems cost >£250k, use mirrors for optics and mechanically raster a single pixel. A further limitation of existing commercial systems is the time taken to produce an image from the mechanically rastered single pixel detector, taking minutes to hours to compile detailed images. IR focal plane arrays, typically comprising array sizes of 640x320 pixels read out at 30 Hz, have been used for THz imaging applications[26] however these sensors have less than 5% absorption in the THz region and do not provide sensitive enough detection. Integration of our single band or

broadband THz metamaterial absorber with a thermal sensor, such as a pn diode or resistive bolometer, into a focal plane array would realize a device capable of absorbing 80% of the THz radiation at the resonance frequency. Such a device would provide a highly sensitive, frequency selective, real time, compact, room temperature THz imaging sensor.

Disclosures

No conflicts of interest declared.

Acknowledgements

References

1. Pendry, J.B., Holden, A.J., Robbins, D.J., & Stewart, W.J. Magnetism from conductors and enhanced nonlinear phenomena. *IEEE Trans. Microw. Theory.* **47**, 2075-2084 (1999).
2. Pendry, J.B., Holden, A.J., Robbins, D.J., & Stewart, W.J. Magnetism from conductors and enhanced nonlinear phenomena. *IEEE Microw Theory*. **47**, 2075-2084 (1999).
3. Smith, D.R., Padilla, W.J., Vier, D.C., Nemat-Nasser, S.C., & Schultz, S. Composite medium with simultaneously negative permeability and permittivity. *Phys. Rev. Lett*. **84**, 4184-4187 (2000).
4. Dolling, G., Wegener, M., & Linden, S. Realization of a three-functional-layer negative-index photonic metamaterial. *Opt. Lett*. **32**, 551-553 (2007).
5. Zhang, S., *et al.* Experimental demonstration of near-infrared negative-index metamaterials. *Phys. Rev. Lett*. **95**, 137404 (2005) .
6. Linden, S*., et al.* Magnetic response of metamaterials at 100 terahertz. *Science*. **306**, 1351-1353 (2004).
7. Landy, N.I*., et al.* Design, theory, and measurement of a polarization-insensitive absorber for terahertz imaging. *Phys. Rev. B*. **79**, 125104 (2009).
8. Gokkavas, M*., et al.* Experimental demonstration of a left-handed metamaterial operating at 100 GHz. *Phys. Rev. B*. **73**, 193103 (2006).
9. Smith, D.R. & Kroll, N. Negative refractive index in left-handed materials. *Phys. Rev. Lett*. **85**, 2933-2936 (2000).
10. Wiltshire, M.C.K, *et al.* Microstructured magnetic materials for RF flux guides in magnetic resonance imaging. *Science*. **291**, 849-851 (2001).
11. Pendry, J.B. Negative refraction makes a perfect lens. *Phys. Rev. Lett*. **85**, 3966-3969 (2000).
12. Kabashin, A.V., *et al.* Plasmonic nanorod metamaterials for biosensing. *Nat. Mater.* **8**, 867-871 (2009).
13. Dolling, G., Enkrich, C., Wegener, M., Soukoulis, C.M., & Linden, S. Low-loss negative-index metamaterial at telecommunication wavelengths. *Opt. Lett.* **31**, 1800-1802 (2006).
14. Schurig, D*., et al.* Metamaterial electromagnetic cloak at microwave frequencies. *Science.* **314**, 977-980 (2006).
15. Chen, H.T. *,et al.* Experimental demonstration of frequency-agile terahertz metamaterials. *Nat. Photonics.* **2**, 295-298 (2008).
16. Ma, Y., Khalid, A., Saha, S.C., Grant, J.P., & Cumming, D.R.S. THz band pass filter on plastic substrates and its application on biological sensing. *IEEE Photonics Society Winter Topicals Meeting Series.*, 50-51 (2010).
17. Grant, J., *et al.* Polarization insensitive terahertz metamaterial absorber. *Opt. Lett.* **36**, 1524-1526 (2011).
18. Ma, Y., *et al.* A terahertz polarization insensitive dual band metamaterial absorber. *Opt. Lett.* **36**, 945-947 (2011).
19. Grant, J., Ma, Y., Saha, S., Khalid, A., & Cumming, D.R.S. Polarization insensitive, broadband terahertz metamaterial absorber. *Opt. Lett.* **36**, 3476-3478 (2011).
20. Tonouchi, M. Cutting-edge terahertz technology. *Nat. Photon.* **1**, 97-105 (2007).
21. D. Schurig, J.J.M., Justice, B.J., Cummer, S.A., Pendry, J.B., Starr, A.F., & Smith, D.R. Microwave Cloaking Realized. *Science.* **314**, 889 (2006).
22. Padilla, W.J., *et al.* Electrically resonant terahertz metamaterials: Theoretical and experimental investigations. *Phys. Rev. B.* **75**, 041102 (2007).
23. Smith, D.R., Vier, D.C., Koschny, T., & Soukoulis, C.M. Electromagnetic parameter retrieval from inhomogeneous metamaterials. *Phys. Rev. E.* **71**, (2005).
24. Landy, N.I., Sajuyigbe, S., Mock, J.J., Smith, D.R., & Padilla, W.J. Perfect metamaterial absorber. *Phys. Rev. Lett.* **100**, 207402 (2008).
25. Hao, J.M., *et al.* High performance optical absorber based on a plasmonic metamaterial. *Appl. Phys. Lett.* **96**, 251104 (2010).
26. Chen, H.T. Interference theory of metamaterial perfect absorbers. *Opt. Express.* **20**, 7165-7172 (2012).
27. Lee, A.W.M. & Hu, Q. Real-time, continuous-wave terahertz imaging by use of a microbolometer focal-plane array. *Optics Letters.* **30**, 2563-2565 (2005).
28. Thermo Nicolet Corporation, An Introduction to Fourier Transform Infared Spectroscopy., (2001).